Astron. Astrophys. 310, 661–671 (1996)

ASTRONOMY AND ASTROPHYSICS

The height distribution of non-thermal X-ray sources in impulsive solar flares

Lyndsay Fletcher*

Sterrekundig Instituut, P.O.Box 80000, 3508 TA Utrecht, The Netherlands

Received 28 February 1995 / Accepted 13 November 1995

Abstract. In this paper we use numerical simulations to accurately model the evolution of non-thermal electron distributions in coronal loops, from which we calculate electron bremsstrahlung height versus energy distributions. The results are compared with results of the Yohkoh satellite and it is found that a model taking into account the full complexity of electron transport can explain what is observed, for quite reasonable loop parameters. We test three loop models, the first with no field convergence, the second with field convergence occurring rapidly and only in the chromosphere and the third where field convergence occurs slowly in the corona. We demonstrate the effects of varying parameters of the loop (such as density, length and field strength), and of the beam (spectral index, pitch angle distribution) and outline parameter regimes in which best agreement with the data can be found. Broadly, densities between 2×10^{10} and $3 \times 10^{11}\mathrm{cm}^{-3}$ and coronal half-lengths L $= \sim 1.3 - 2.7 \times 10^{9}$cm give qualitatively acceptable results. Finally we discuss possible tests to distinguish between the various models which can explain the height distribution.

Key words: sun:X-rays; corona; flares

1. Introduction

Acceleration processes during solar flares result in non-thermal particles moving into interplanetary space along open magnetic field lines and towards the chromosphere along the loop legs. An important observational signature of these accelerated electrons is coronal and chromospheric hard X-ray (HXR) emission, and recent developments in instrumentation have enabled the sites of this emission to be studied in considerable spatial and temporal detail.

We here address one of the large number of questions raised by recent results from the Yohkoh Satellite - the spatial distribution of HXR sources in the solar atmosphere. Matsushita et al. (1992) report that the mean position of HXR emission observed with the Hard X-ray Telescope (HXT) decreases as HXR photon energy increases. They also propose that the X-ray emission may originate from two components, a super-hot thermal source near the top of the loop (of $\sim 10^8$ K, needed to produce 10's of keV HXR), and a thick-target source located at the loop footpoints, and claim that the observations rule out the possibility that electrons are trapped in coronal loops, but are supportive of electron precipitation without trapping, given a high density throughout the loop. We shall address the trap-plus-precipitation model using a numerical simulation to properly model trapping and scattering processes. In agreement with Matsushita's proposal, we find that if a high loop density is invoked, the pure precipitation model gives agreement with observations, but also that the 'trap-plus-precipitation' model is consistent with the observational findings for the kind of low loop density inferred from soft X-ray (SXR) observations of impulsive flare loops. We thereby demonstrate that the observations are consistent with partial electron trapping, (which is an inevitable consequence of magnetic field convergence).

1.1. Observational background

Recently the Japanese Yohkoh satellite (Ogawara et al. 1991) has provided the solar community with spatially and temporally resolved images of the sites of solar flare X-ray emission, revealing a multitude of different types of flare behaviour and a marvellous complexity of dynamical structures in active regions. But despite these new observations, ideas about the basic flare structure remain little changed. Overlays of HXR and Soft X-ray (SXR) images (Sakao 1994) provide fairly conclusive evidence that a coronal magnetic loop, or arcade of loops, rooted in the lower atmosphere, defines the geometry in which the flare occurs, and evidence for the presence of double footpoint HXR structures, implying emission from the footpoints of a loop, is now rather convincing. Sakao et al. (1994), using the Hard X-ray Telescope onboard Yohkoh (Kosugi et al. 1991) have found double or multiple footpoints in 70% of flares (exceeding a certain count-rate in the 33-55 keV energy band), which, they suggest, is not likely to be due to a chance coincidence of single sources, but

* now at Solar System Division, Space Science Department, ESTEC, Postbus 299, 22 AG Noordwijk, The Netherlands

indicative of emission from footpoints of connected magnetic loop structures. The remaining single sources they interpret as unresolved double sources or cases in which the emission from one footpoint is too weak to be observed.

The variety of SXR and HXR spatial and temporal behaviour has proved to be wide, with a number of new classifications of source structures. But whilst the X-ray flare zoo grows there are still useful statistical studies to be made on the global properties of flares, within a given broad classification (eg, 'impulsive' as opposed to 'gradual'). One such study was carried out by Matsushita et al. (1992), who, using Hα flare locations and Yohkoh observations in 4 energy channels, determined the mean location of HXR sources as a function of energy. It was found that, relative to the top of the photosphere, the mean source position in the L band (13.9-22.7keV) is $(9.5 \pm 2) \times 10^3$ km. The sources in the M1 (22.7-32.7), M2 (32.7 - 52.7) and H (52.7 - 92.8) bands are respectively $(1.0 \pm 0.3) \times 10^3$ km, $(2.0 \pm 0.5) \times 10^3$km and $(3.2 \pm 0.7) \times 10^3$ km *below* the L band source.

Previous imaging work on the heights of X-ray sources (Takakura *et al.* 1986) with the Hinotori imager found that a source in the 40-60keV range originated at $(7 \pm 3.5) \times 10^3$km, consistent with the Matsushita et al. result. Using stereoscopic measurements Kane (1983) estimated that 95% of $\sim$ 150keV emission, in 3 impulsive flares, came from below 2500km above the photosphere.

1.2. Trapping and precipitation in the coronal loop

We consider the motion of non-thermal electrons in a coronal magnetic trap, subject to Coulomb collisions with the ambient medium, and to the magnetic mirror force (in regions of non-uniform field). This problem has already been studied by a number of authors, analytically and numerically, starting with Kane (1974), and Melrose and Brown (1976). Analytical work (eg MacKinnon 1988, Alexander 1990, Hulot et al. 1992) is limited by the complexity of the evolution Eq. (see 1), and in general many assumptions must be made to permit a solution. For example, one normally assumes that the field convergence between corona and chromosphere occurs in a very short distance and at the position of a similarly abrupt change between coronal and chromospheric densities. The first assumption allows a 'loss-cone' to be well defined (the region in pitch-angle space from which, once they have entered it, particles are assumed to precipitate and be lost from the coronal population), whilst the second means that particles in the loss-cone are indeed precipitated and lose their energy via collisions before being able to mirror. Such assumptions make the analytical treatment of the problem possible, but need not be satisfied. In general, the scattering and mirroring processes happen co-spatially. A loss-cone must then be defined throughout the loop as a function of position and energy. In addition, particles are scattered in or out of the loss-cone by Coulomb collisions, a process which also depends on the particle energy and the loss-cone size. Such complications make a full analytic solution impossible.

The alternative is to solve the evolution equation fully by numerical means. The relevant equation for the particle density distribution is the Fokker-Planck equation, which, if Coulomb scatterings and magnetic mirroring are the predominant scattering and loss terms, is

$$\frac{\partial f}{\partial t} + \mu v \frac{\partial f}{\partial S} - m_e D(S) \frac{\partial}{\partial E}\left(\frac{f}{v}\right) - \frac{D(S)}{v^3 \gamma^2} \frac{\partial}{\partial \mu}\left((1-\mu^2)\frac{\partial f}{\partial \mu}\right)$$

$$-\frac{v}{2}\frac{\partial}{\partial \mu}\left((1-\mu^2)\frac{dlnB}{dS} f\right) = s(t, S, v, \mu) \qquad (1)$$

where the coefficient $D(S)$ is given by

$$D(S) = \frac{4\pi e^4 n(S) \Lambda(S)}{m_e^2} \qquad (2)$$

(Hamilton et al. 1990). Λ is the Coulomb logarithm (eg Emslie 1978) and $n(S)$ the ambient loop density. Equation (1) is in the general form for electrons of velocity v, $\mu = \cos\theta$ where θ is the particle pitch angle (the angle between its direction of travel and the local field direction) and total energy $E = (\gamma - 1) m_e c^2$ ergs. (Note that in Hamilton *et al* (1990) energy is quoted in units of $m_e c^2$ - our energy expressions are therefore somewhat different from theirs.) S is the distance along a magnetic field line measured from the loop apex, and s is the source function. Equation 1 is correct if there are no significant cross-field terms, so that position is completely defined by a length co-ordinate along a field line and a pitch angle. We must also be in the limit where the change in particle momentum due to individual scatterings is much less than the original particle momentum and. With these constraints obeyed, (1) adequately describes the case of Coulomb collisions of non-thermal electrons.

In Eq. 1 there is no term to model the effect of deceleration in the electric field of a return current, or by anomalous resistivity, so the applicability of our model is limited to the regime in which Coulomb collisions dominate, which depends on the ratio of the beam density, here n_b to the ambient density n, and on the ambient electron temperature. According to van den Oord (1990) the primary energy losses are collisional if $v < (n_b/n)^{1/3} v_{th}$ and anomalous resistivity sets in if $v > (n_b/n) c_s$ where n_b is the beam density, v_{th} is the electron thermal speed and c_s is the ion acoustic speed = $(kT/m_i)^{1/2}$. If we assume that the total energy released in the flares associated with looptop sources is 10^{31} ergs (reasonable for M-type flares, as the observed flares are), over a timescale of 5 minutes and assume also that the majority of this energy is in the form of a beam which covers a chromospheric area of 10^{18}cm^2 this gives an energy flux of 3.3×10^{10}ergs cm^{-2}s^{-1}. If there is a power-law distribution of electrons extending from 20keV to infinity, then the required beam density is a few times 10^8 electrons cm^{-3}, for flux power-law indices between 3.5 and 6.5. Therefore, for the ambient densities which we shall consider, $3 \times 10^{10} - 3 \times 10^{11}$ electrons cm^{-3}, the beam (20 - 200 keV) is in the Coulomb collision-dominated regime for plasma temperatures of a few times 10^7 K, which is quite reasonable for coronal plasmas.

McClements (1990) solved Eq. 1 using a finite difference integration method, in the case where field convergence occurs

in the corona, in a uniform density region. This choice of field was justified on the grounds that if convergence occurred lower down, in the chromosphere, all particles would lose their energy via scattering, before being able to mirror. Whether or not this is the case evidently depends on particle energy, and the manner in which the field converges. We will investigate the radiation emitted from two classes of trap models - one being the coronal convergence case as described by McClements (1990) and a second where the field convergence occurs in the chromosphere, where density is increasing rapidly. In addition, results from a calculation without trapping are considered.

The paper is organised as follows. In Sect. 2 we describe briefly our numerical technique and provide a test against an analytic solution. Sect. 3 describes the models which we take for the solar chromosphere and corona, and the form for our electron source term and boundary conditions and Sect. 4 the calculation of HXR intensity and the mean HXR source height from the electron distribution. The results are compared with observations in Sect. 5 and suggestions made for distinguishing between the allowable models in Sect. 6. In Sect. 7 some conclusions are drawn about the viability of the models and permissible parameter regimes.

2. The numerical simulations

We find numerical solutions to Eq. 1 using the method of stochastic simulations. This method was introduced in an astrophysical context by MacKinnon and Craig (1991) who pointed out its usefulness in dealing with diffusion of fast electrons and indicated the reliability of the model by testing against a restricted class of numerical solutions of the diffusive Fokker-Planck equation, without magnetic field convergence terms. We here include magnetic convergence effects. Below the implementation is briefly described.

Mathematically it can be demonstrated (eg, Gardiner 1985) that a Fokker-Planck equation in the form

$$\frac{\partial f}{\partial t} = -\frac{\partial}{\partial x_i}(A_i f) + \frac{1}{2}\frac{\partial^2}{\partial x_i \partial x_j}(B_{ij} f) \tag{3}$$

is formally equivalent to the set of stochastic differential equations

$$d\underline{x} = \underline{\mathbf{A}}(\underline{x}, t)dt + \underline{\underline{\mathbf{B}}}^{\frac{1}{2}}(\underline{x}, t)d\underline{\mathbf{W}}(t) \tag{4}$$

which describes the path of a single particle under the influence of advective and diffusive terms $\underline{\mathbf{A}}$ and $\underline{\underline{\mathbf{B}}}$. The random walk nature of pitch-angle scattering means that the result of a large number n of actual, physical scatterings, taking a total time Δt to occur is a variable distributed with a Gaussian distribution, variance $(2\Delta t)^{1/2}$. The cumulative change in pitch-angle of a typical particle after n scatterings taking time Δt is then given by an (appropriately scaled) number drawn from such a Gaussian. This is $w(t)$ in Eq. 5 below. A sufficiently large number of realisations of individual particle orbits allows us to generate distribution functions for particle phase-space co-ordinate.

For Eq. 1 the stochastic differential equations, in their relativistic form, are as follows.

$$\begin{aligned} dS &= \mu\beta c dt \\ d\gamma &= \frac{-4\pi e^4 \Lambda n}{m_e^2 c^3 \sqrt{(1-\gamma^{-2})}} dt \\ d\mu &= \left[\frac{-8\pi e^4 \mu \Lambda n}{m_e^2(\beta c)^3} - \frac{\beta c}{2}(1-\mu^2)\frac{dlnB}{dS}\right] dt \\ &+ \left[\frac{4\pi e^4 \Lambda n}{m_e^2}\frac{(1-\mu^2)}{(\beta c)^3}\right]^{1/2} w(t) \end{aligned} \tag{5}$$

with $\beta = v/c$ and $\gamma = (1-\beta^2)^{-1/2}$. As pointed out by MacKinnon and Craig (1991), once the drift and diffusion coefficients for the process under study are known, no other physical input is necessary to simulate particle transport. These coefficients are in general dependent on spatial and velocity co-ordinates of the test particle and so require to be continually updated as the calculation progresses. This can be achieved easily in the stochastic simulation.

There are no source terms in Eqs. 5, however the source is implicit in our calculations. In Eq. 1 s represents mathematically the form of the distribution function at injection. We, however, solve only the motion of the particles, so we put $s = 0$ in (1) for the formal solution by the stochastic method and the source term enters via the real distribution function of the numerical particles which are injected and followed through the system.

The equations are solved stepwise, starting with the energy equation. The timestep used in the solution must in general be chosen keeping in mind the length scales associated with the advective terms in the F-P equation - for example the length scale on which the magnetic field convergence occurs. If $v\Delta t$ is greater than this scale then on average a particle never gets a chance to 'interact' with the structure. The diffusion term has no such definite length scale: as described above the change in pitch-angle after time Δt follows a Gaussian distribution, and if Δt is large so that particles only experience a few 'scatterings' over their entire trajectory, then we have only to increase the number of trajectories simulated to improve the statistics on the resulting distributions.

To test the numerical method we follow McClements (1990) and compare the results of the simulations with an analytic solution available for the case of a highly beamed injection in a uniform, pure scattering atmosphere, given by Leach & Petrosian (1981). If the injected particles have a density distribution given by

$$f(v, \mu = \cos\alpha)_{S=0} = N_0 \left(\frac{E}{E_0}\right)^{-\delta} \frac{2}{\alpha_0^2} e^{-\alpha^2/\alpha_0^2}, \tag{6}$$

then the solution for small pitch-angles is

$$f(v, \mu, S) = \frac{N_0 \left(\frac{E}{E_0}\right)^{-\delta} 2e^{-2(1-\mu)/(\alpha_0^2 + 4ln(v_c/v))}}{\alpha_0^2 + 4ln(v_c/v)} \tag{7}$$

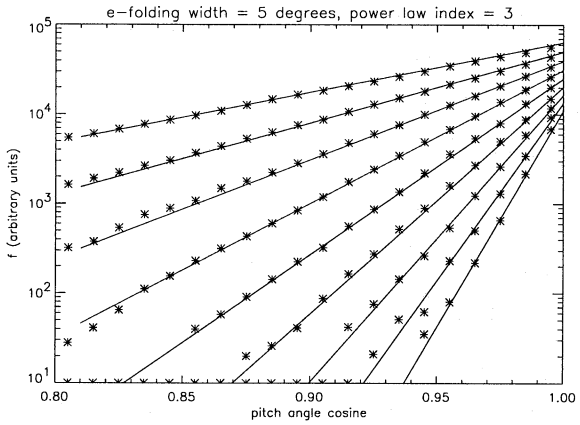

Fig. 1. A test run of the stochastic simulation (asterisks) versus analytic results. The uppermost line corresponds to an electron velocity of 7.86×10^9cm s^{-1}, thereafter the increase is 1.05×10^9cm s^{-1} per line.

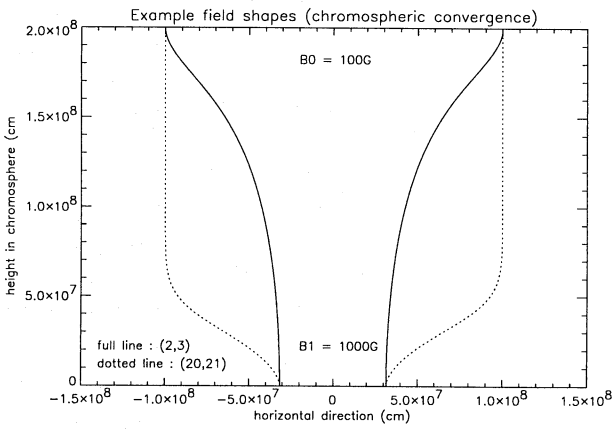

Fig. 2. Representative field shapes. Here the field converges entirely within the chromosphere and the tube radius at the surface is 10^8cm. The bracketed figures refer to the (p_1, p_2) values used in Eq. (8)

Here $v_c = (v^4 + 4DN(S))^{1/4}$ where $N(S)$ is the column depth at S. For very small α, $\alpha^2/2 = 1 - \mu \ll 1$ where μ is the pitch-angle cosine, and the injected distribution function is then almost a Gaussian in pitch-angle, and is very narrow, with e-folding width α_o. We compare the results of numerical simulations with the analytic solution for $\mu > 0.8$, as did McClements(1990). We have chosen an e-folding half-width of 2.5° a power-law index in energy of 3.5, and a cut-off at low energy at 20keV. We examine the distribution at a column depth of 3×10^{19}cm^{-2} in an atmosphere with a uniform density of 10^{10}cm^{-3} .

As can be seen from figure 1 the agreement between the numerical and analytical results is satisfactory. At higher velocities and higher pitch-angles the relatively small number of particles per bin increases the scatter of the numerical points. On any particle bin population N there will be $\sqrt{N}$ counting noise. The relative error decreases as the number of particle runs is increased.

Having demonstrated once more the viability of the stochastic simulation method, we may proceed to the more complex case of convergent magnetic field and varying atmospheric density.

3. The models

3.1. The magnetic field and density structure

Although convergence of the magnetic field of a coronal loop between the loop-top and some location in the chromosphere is very likely, for comparison we calculate also the case of no convergence - the pure thick-target precipitation model (Sect. 5.1). Following this we model trapping utilising 2 classes of field convergence - chromospheric (Sect. 5.2) and coronal (Sect. 5.3). There is possibly more evidence for convergence in the chromosphere. Observationally Yohkoh SXR images (e.g., Dennis et al. 1994) have shown compact coronal loops which appear to be rather uniform in cross-section (if one assumes that the SXR emitting material is constrained by the magnetic field), therefore the strengthening of the field between corona and photosphere must occur at some point in the chromosphere. Theoretically, quiet sun flux-tube models of Solanki & Steiner (1990) give convergence in the chromosphere (at about 1400-1700km if the material in the flux tubes is heated to a temperature higher than the surroundings, but lower down if inside and outside the tube are at the same temperature). However, the probable variety of field forms demands that we should also examine a representive coronally convergent case.

An analytic form for a magnetic field convergent in the chromosphere is given in MacKinnon & Brown (1990). Coordinate S, has values S_0 and S_1 at the top and bottom of the chromosphere respectively. The coronal field is uniform with value B_0 and at the bottom of the chromosphere the field has value B_1. In the chromopshere the field converges according to

$$B_S(S) = B_o + \frac{(B_1 - B_o)}{(p_2 - p_1)}[p_2 x^{p_1} - p_1 x^{p_2}] \quad (8)$$

where

$$x = (|S| - S_o)/(S_1 - S_0) \quad (9)$$

The height and 'sharpness' of convergence are determined by the parameters p_1 and p_2. We consider two cases - rapid convergence high and low in the chromosphere. These field shapes are shown in Fig. 2.

For the case of coronal convergence we use an exponential field, as did McClements (1990). The form for the field is

$$B(S) = B_o e^{S/l} \quad (10)$$

which, as noted by McClements does not have zero divergence, but does have a suitable 'shape' for our purposes. The field scaling parameter l depends on B_o/B_1.

The loop is symmetric and semi-circular and its half-length *in the corona*, L is a variable parameter. There are suggestions (Mandzhavidze & Ramaty 1993 and references therein) that impulsive flares originate in lower-lying loops, with loop-top

heights (not the same as loop-length!) $\lesssim 10^9$ cm whereas gradual and longer lasting flares occur in much larger structures ($\gtrsim 10^{10}$cm). Since the flares in the study of Matsushita et al. are impulsive we consider smaller loops - up to a few times 10^9 cm in length.

Although the convergence of the magnetic field will be in some way related to the changes in ambient pressure throughout the chromosphere, modelling work by Solanki & Steiner (1990) shows that the shape of the flux tube in fact depends also on surface field filling factor, loop temperature stratification and thermal inhomogeneities in the chromosphere, none of which enter our considerations. Therefore we assume that we have the freedom to vary the chromospheric density without changing the field shape, and vice versa.

A glance through the solar physics literature reveals numbers between a few times 10^9 and 10^{12}cm^{-3} appearing as coronal flare loop densities, depending upon the loop size, the type, the size and the phase of the flare. In the SMM classification (Vlahos *et al.* 1984), impulsive flares showing a double footpoint structure were attributed densities of $\lesssim 10^{10}$cm^{-3} . Densities of $\gtrsim 10^{11}$cm^{-3} are usually associated with small volumes or low filling-factors, or with the gradual phase of a flare. We investigate densities of a few times 10^{10-11}cm^{-3} . For simplicity we assume that coronal density is uniform. The chromospheric density varies according to an exponential law

$$n(d) = n_o e^{-d/d_o} \tag{11}$$

where d is the distance up from the bottom of the chromosphere, n_o is photospheric density and d_0 is the chromospheric scale height. Fitting an exponential to the semi-empirical flare model atmosphere F1 of Machado et al. (1980) gives n_o = 9.23×10^{16}cm^{-3} and $d_0 = 1.4 \times 10^7$cm. If we vary the scale height parameter, this changes the chromospheric and coronal density whilst keeping photospheric density fixed. The depth of the chromosphere - i.e., the depth over which the density varies, is constant and equal to 2×10^8 cm.

3.2. Injection Conditions

We consider a non-thermal electron spectrum injected with a low-energy cut-off of 20keV. The spectrum has a power-law in flux, the index of which can be varied in the computations. The power-law spectrum extends in principle to infinite energies, but in practice we cut it off above a certain limit, which is determined by the maximum X-ray energy ϵ_{max} in HXR which is of interest. Photons of energy ϵ_{max} are generated by electrons of $E > \epsilon_{max}$, which have been scattered down from higher energies. We set the upper cutoff E_u in electron energy such that the number of particles with energy between ϵ_{max} and E_u is much greater than the number of particles between E_u and infinity. This ensures that any shortfall in the bin populations caused by the absence of particles which should have been scattered down from $E > E_u$ is kept small. The injected particle number is large enough that particles in high energy bins have $\sqrt{N}/N < 0.1$.

With our method of solution it is possible to study the fully time-dependent solution to the transport equation. However, we instead integrate over time the time-dependent solution obtained from a single injection at $t = 0$, arriving thus at a steady-state solution (Fletcher and Brown 1995). The electrons are injected at $S = 0$ in the corona with pitch-angles in the forward hemisphere. We use three angular distributions - isotropic ($f(\theta)$ distribution uniform), anisotropic and directed predominantly along the field ($f(\sin\theta)$ distribution uniform) and directed predominantly perpendicular to the field ($f(\cos\theta)$ distribution uniform). The distribution evolves along one 'leg' of the symmetric loop, and particles which mirror and travel back past $S = 0$ re-enter the calculation with their velocity reversed in direction. This mimics the effect of having an injected distribution symmetric about $S = 0$ with all particles in one leg being counted, including those which have mirrored and come from the other leg. Particles continue travelling and mirroring in the loop until they have thermal energies, at which point the calculation stops.

4. Calculation of hard X-ray emission

The X-ray differential intensity (photons s^{-1} cm^{-3}) per unit energy, from electron-proton bremsstrahlung is given by

$$I(\epsilon, S) = \int_{\epsilon}^{\infty} f(S, E)\beta(E)cn(S)\sigma(\epsilon, E)dE \tag{12}$$

where $\sigma(\epsilon, E)$ is the cross-section for emission of a photon of energy ϵ by an electron of energy E. We use the non-relativistic Bethe - Heitler cross-section for electrons of energy $\lesssim E_u = 150$ keV,

$$\sigma(\epsilon, E) = \frac{7.9 \times 10^{-26}}{\epsilon E} \ln\left[\frac{1 + (1 - \epsilon/E)^{1/2}}{1 - (1 - \epsilon/E)^{1/2}}\right] \text{cm}^2\text{erg}^{-1} \tag{13}$$

This is the cross-section integrated over the direction of incoming and outgoing photons. In using it we lose all HXR directional information, but as we discuss in Sect. 6 the calculation of directional quantities such as polarisation and directivity may be useful in distinguishing between the models permitted by the height-versus-enery studies.

The result of the numerical simulations is a histogram of $f(E, S)$, rather than functional representation, therefore integral(12) must be performed in a piecewise manner. The population contained in a bin $(S_i, S_{i+1}), (E_j, E_{j+1})$ is attributed to a single location in the geometric centre of the bin, giving a set of values $f(S_{i'}, E_{j'})$. Values of the cross-section and the ambient proton number density are then calculated at $E_{j'}, \epsilon_{k'}$ and $S_{i'}$, and integral 12 is approximated using a fourth order Simpson's rule. The results of this integration, $I(\epsilon, S)$ are then averaged over height to give the mean position $\overline{S}$ along the loop of the source.

$$\overline{S}(\epsilon) = \frac{\int_h I(\epsilon, S) S dS}{\int_h I(\epsilon, S)} \tag{14}$$

This is not however the height of the source, since the loop is curved (semicircular in our assumption). $\overline{S}$ is converted to $\overline{h}$, the height above the chromosphere. The variation of $\overline{h}$ with ϵ is compared with the observed variations.

5. Comparison of theoretical results with observations

With the results presented in this paper we shall easily be able to show that our non-thermal model can give agreement with the observations. In the following sections, we vary the loop length and density, the magnetic field strengths and shape, the injected power-law index and the angular distribution of the beam, in the context of three different magnetic scenarios, and examine the resulting distributions. However, at this stage the conclusions which we draw from our modelling are not very detailed, since the number of adjustable parameters in the problem exceeds the number of data points. For this reason we shall consider in a following section other ways in which the various models could be distinguished.

In considering the models below, we will define 'an acceptable fit' as one in which the calculated distribution of height with energy passes through all four of the boxes defined by the error bars on the data points. A possible extension to this 'eyeball' analysis would be the calculation of the χ^2 goodness-of-fit parameter, for many different values of the loop and beam parameters, however with only 4 data points it is not clear that this would yield any more useful information than one gets from simply looking at the plot.

5.1. Non-trapping models

As is stated in Matsushita et al. the decrease in height with increasing X-ray energy arises also in thick-target calculations not involving trapping. With semi-empirical chromosphere/corona models, Brown and McClymont (1975) calculated heights of less than 5km above the photosphere for HXR sources. The smallness of this value compared to the present observations is due to two factors. Firstly, a quiet sun chromospheric and coronal model is used which is very probably underdense compared to the situation during a flare, and secondly the treatment used is greatly simplified in terms of its neglect of particle scattering and magnetic effects. MacKinnon & Craig (1991) demonstrated that the use of even the next step up from thick-target beam model, the mean-scattering treatment, gives inadequate results even for the 'gross consequences' of particle transport, such as where the majority of electron energy is deposited and how the pitch angle and energy distribution evolves with position. For example, they find that in the case of a beamed injection, the stochastic method shows substantial energy deposition occuring at column depths greater than the mean-scattering value for the stopping depth - in other words, at positions where a mean-scattering treatment predicts no particles, there are in fact particles present. From this we infer that the rate of energy loss with position is smaller in the full scattering treatment than in the mean-scattering treatment. The consequence of this is a greater number of HXR photons emitted, and higher up, than the simple beam, or mean scattering model could predict, and we expect to see in our results that HXR emission comes from considerably higher up than in the model presented by Brown and McClymont.

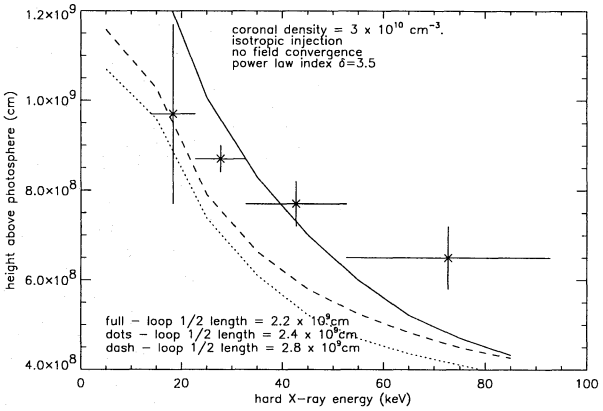

Fig. 3. The variation of mean X-ray emission height with energy. The points are the observational data of Matsushita *et al* and the curves are models with coronal loop lengths, as indicated on the diagram. The horizontal error bars are the energy bin widths whilst the vertical error bars are the 1σ errors quoted by Matsushita *et al.* Density is kept constant at $3 \times 10^{10}\mathrm{cm}^{-3}$ and the injected distribution is isotropic. In these simulations a uniform magnetic field is used.

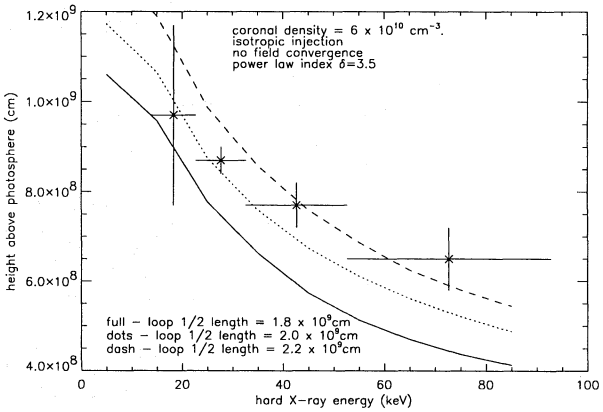

Fig. 4. As Fig. 3 but with $\rho = 6 \times 10^{10}\mathrm{cm}^{-3}$.

Below we present some results which illustrate attempts to fit the observations by a simple thick-target model, and show the effect of varying the parameters involved in the calculation.

The effect of varying loop-length and density.
Changing the loop length and density both amount to changing the column depth traversed by the electrons, however the effects must be separated. Increasing the loop length shifts upwards the mean position of emission at a certain energy, simply because injection takes place higher up in the corona but increasing the density compresses the length-scale of energy loss in the medium. This also has the effect of moving upwards the mean emission position. In Figs. 3 to 5 we show, superimposed on the data points of Matsushita et al. a few different curves, for which density and length are varied, and other parameters held constant. The power-law index was $\delta = 3.5$ and the injection was isotropic over pitch-angle.

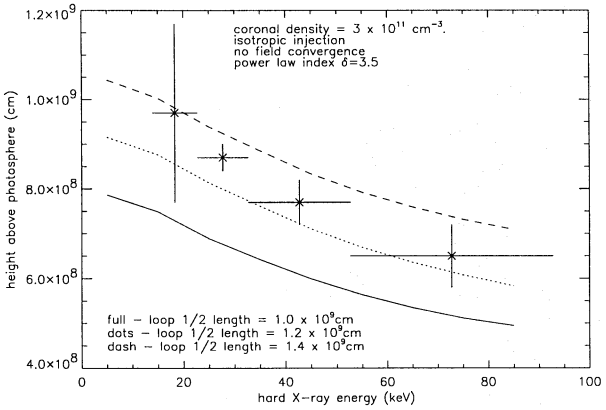

Fig. 5. As Fig. 3 but with $\rho = 3 \times 10^{11}\mathrm{cm}^{-3}$.

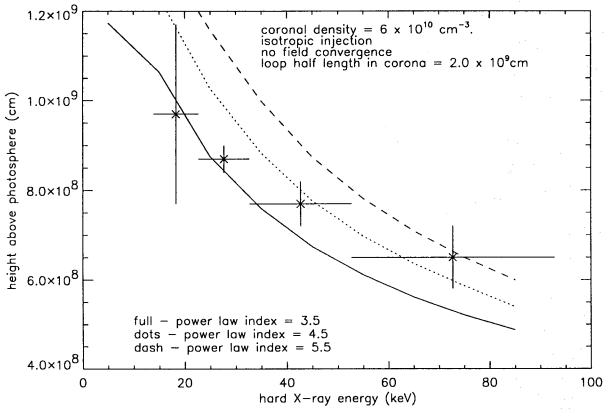

Fig. 6. $\rho = 6 \times 10^{10}\mathrm{cm}^{-3}$, coronal loop half-length = 2.0×10^9 cm, isotropic injection. The power-law index is varied.

Note that in Fig. 3, although the upper solid line does formally pass through the error boxes defined by the observational points, the deviation from them is considerably larger than in either of Figs. 4 or 5 and by eye is much less convincing a fit than the best lines of these two cases. Lower densities steepen the theoretical curves too much to give satisfactory agreement. The highest loop density giving an acceptable fit was $3 \times 10^{11}\mathrm{cm}^{-3}$. For any given value of loop density there is evidently a range in loop length which gives agreement, which is in fact rather restricted - typically a range of 2×10^8cm.

The effect of changing the injected energy and pitch angle distribution

As can be seen in Fig. 6, increasing the δ of the injected distribution results in an increase in mean source-height. This can be explained in the following way. HXR emission of an arbitrary energy ϵ is only generated by electrons of energy greater than ϵ. If we consider this 'tail' distribution of electrons which can generate HXR photons of energy ϵ to be represented by a single electron of the mean energy, it can be seen that since this mean energy is higher for a harder spectrum, so the typical column depth over which the tail is 'emptied' by collisions is greater for a harder spectrum. This means that a greater proportion of the

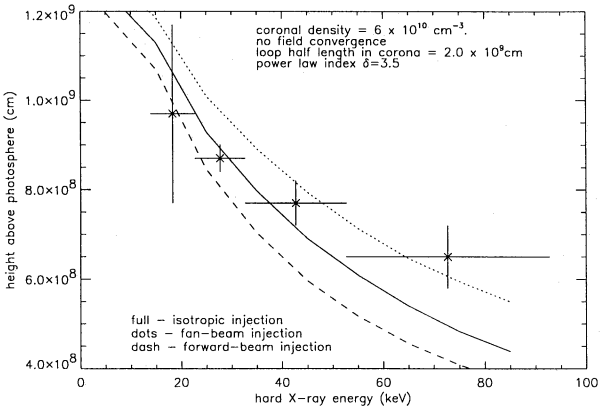

Fig. 7. $\rho = 6 \times 10^{10}\mathrm{cm}^{-3}$, coronal loop half-length = 2.0×10^9 cm, power-law index = 3.5.The shape of the injected distribution is varied.

electrons from the hard spectrum attain the chromosphere, and since density increases rapidly here this weights the emission more towards lower altitudes, resulting in a lower mean height for emission at energy ϵ.

Changing the shape of the injected distribution also has a marked effect on the curves obtained, on both their position and gradient. One example of this is given in Fig. 7. Increasing the pitch-angles of electrons in a distribution (i.e., a fan-beam distribution as opposed to an isotropic or beam distribution) also leads to a shorter column depth for energy loss at a given initial energy, and this affects the distribution in the same way as described in the above paragraph, by weighting the distribution of HXR emission towards higher altitudes in the case of a shorter energy-loss column depth. However there is a second factor - this being simply that high initial pitch-angle electrons stay near the top of the loop for longer (streaming motions are not along the loop). The differences are more evident at high HXR energies since high energy electrons, having undergone fewer scatterings, retain more the initial angular characteristics of the injected distribution. The injected angular distribution is as yet an unknown quantity, and evidently has an important role in determining the spatial distribution of HXR emission. The most expedient way of studying the angular distribution would be via observations of the polarization of loop radiation. We make some comments on this in a later section.

From the results presented it can be seen that it is possible to obtain a fit to the data for a model with no field convergence, if a high enough density is used. We have seen in addition that changing the power-law index or the shape of the injected distribution is at least as important as is changing parameters of the loop. This underlines the need for alternative tests of the models.

5.2. Convergence within the Chromosphere

Again we present here a selection of the results, with the aim of indicating that trapping of electrons in a field convergent in the chromosphere is consistent with the observational data. In

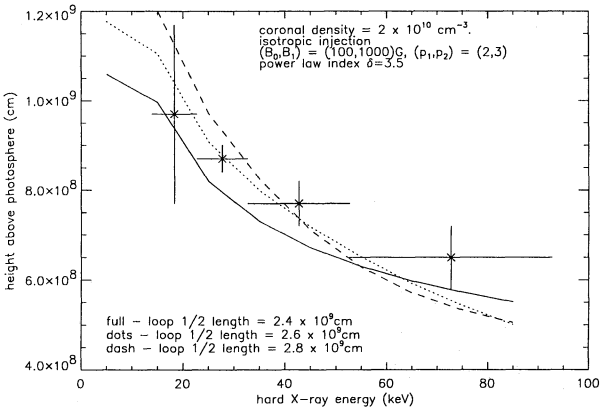

Fig. 8. Models generated with magnetic field converging high in the *chromosphere* (see Fig. 2). $\rho = 2 \times 10^{10}\mathrm{cm}^{-3}$, $\delta = 3$. The curves correspond to various values of coronal loop half-length.

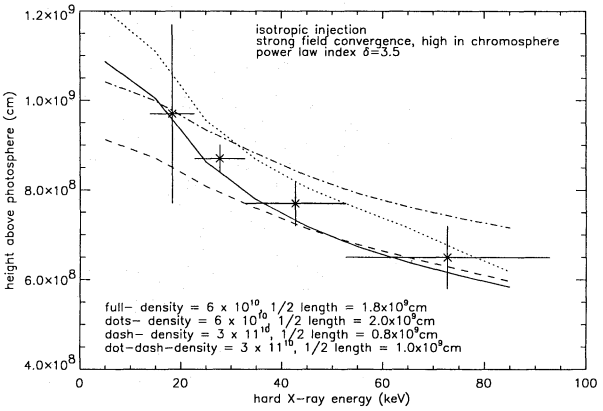

Fig. 9. As Fig. 8 but with $\rho = 6 \times 10^{10}\mathrm{cm}^{-3}$ and $\rho = 3 \times 10^{11}\mathrm{cm}^{-3}$.

addition we discuss briefly the effects of changing the magnetic parameters of the model. In this model the variable field parameters are the photospheric and coronal field values (B_1, B_0) and two parameters which describe the rapidity and position of field convergence, (p_1, p_2). Roughly, at a low p_1, the convergence position is near the top of the chromosphere, and moves down as p_1 increases. A low p_2 corresponds to a gentle convergence and a high p_2 to a very rapid convergence.

Firstly we show curves calculated for a variety of density and length parameters (Figs. 8 and 9), and see from this that also at low densities it is possible to find agreement with the observational information. The lowest density for which an acceptable fit can be obtained is $2 \times 10^{10}\mathrm{cm}^{-3}$, somewhat lower than was found in the non-converging case. This approaches the values associated with compact, double footpoint flare impulsive loops (see Sect. 3.1). Once again the loop density determines a suitable loop length to within 2×10^{8}cm. Note that in Fig. 8 a limit is reached whereafter an increase in loop length is no longer effective in increasing the mean source height. This happens when the coronal column density becomes too great for mirroring particles to return to the loop-top.

Varying field convergence

The two sets of parameters (p_1, p_2) used correspond to high and low convergence positions in the chromosphere, as shown in Fig. 2. Changing these and the absolute field strengths (B_0, B_1) changes trapping efficiency. We first vary (p_1, p_2), with $(B_0, B_1) = (100, 1000)$, an isotropic injection, $\mathrm{L} = 1.9 \times 10^{9}$cm and $\rho = 6 \times 10^{10}\mathrm{cm}^{-3}$. In Fig. 10, the full and the dashed line have the same field strengths but different convergence positions. A particle entering a field which converges low in the chromosphere (here with parameters $(p_1, p_2) = (20, 21)$ in Eq. 8) will on average traverse a larger chromospheric column depth than a particle of the same energy entering a field which converges high in the chromosphere (with parameters $(p_1, p_2) = (2, 3)$), since it mirrors over a longer distance, in a medium where the density increases with depth. The HXR emission from the chromosphere if there is a high convergence position is then a larger fraction of the total than if there is a low convergence position, and the emission is in general weighted towards lower altitudes. At low energy this effect will not be so apparent, since at low energy particles will probably be collisionally stopped before they mirror, and will traverse more-or-less the same column depth (with a correction for the different collisional losses caused by variations between the pitch-angle distributions resulting from field changes). At energies above about 60keV the field shape in the chromosphere is potentially very important in determining the distributions of precipitating *and* trapped electrons. Note that analagous to the case of $>$ 10MeV γ-ray bursts studied by MacKinnon & Brown (1989,90) we might expect that the shape of the magnetic field might affect the distribution of chromospheric HXR bursts, and may also aid us in distinguishing between chromospheric and coronal convergence cases (see Sect. 6)

Varying field ratio

We now change from $B_{chr}/B_{cor} = 10$ to $B_{chr}/B_{cor} = 4$. Compare the full and dotted lines, or the dash and dot-dash lines in Fig. 10. Increasing the 'mirror ratio' improves the trap efficiency. In the simplistic 'loss cone' description, the size of the loss cone decreases, meaning that fewer particles precipitate. In our treatment this happens also and the lower precipitation flux (fewer particles deep in the chromosphere) again means than the emission at all energies is less weighted towards low altitudes, with the effect being more important at high energy.Thus $\overline{h}(E)$ is again somewhat lower.

Shape of injected beam and power-law index

For completeness we also include the effect of changing beam-shape and power-law index. We use a field with parameters $(B_0, B_1) = (100, 1000)$, $(p_1, p_2) = (2, 3)$, and loop density $\rho = 6.0 \times 10^{10}\mathrm{cm}^{-3}$. Fig. 11 shows the effect of changing the shape of the injected spectrum. The shape of the injected distribution is more important here than in the non-trapping case, since escape from the loop is determined in part by the particle pitch-angle. In fact, at this loop density the height-versus-energy distribution is more affected by possible variations in the pitch-angle distribution than it is by reasonable changes in magnetic field. If we vary the power-law index this has the same kind of

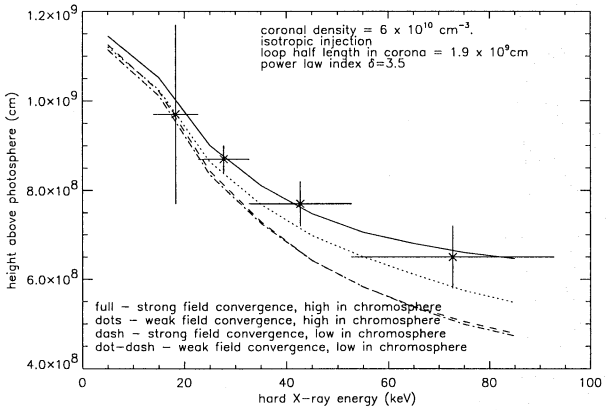

Fig. 10. The effect of changing the convergence position and field - strength. All field convergence takes place in the *chromosphere*.

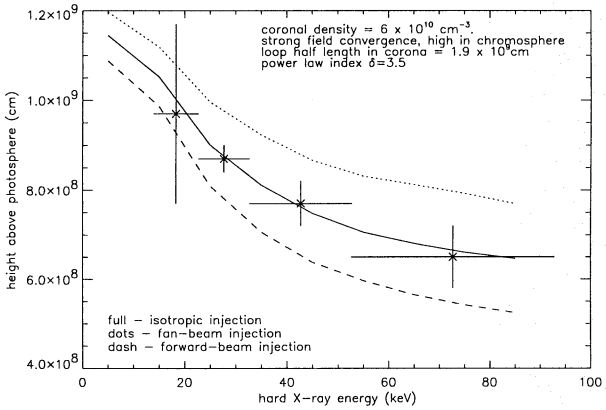

Fig. 11. The effect of changing the form of the injected distribution. All field convergence takes place in the *chromosphere*.

effect as in the no-convergence case. Overall we see that in the case of field convergence we are able, relatively easily, to find curves which pass comfortably through the error bars on all four points, also at low densities.

5.3. Convergence within the corona

We here use the exponentially varying form of field as described in Sect. 3.1, and present results for densities between $3\times10^{10}\mathrm{cm}^{-3}$ and $3\times10^{11}\mathrm{cm}^{-3}$. Once again it can be seen (in Fig. 12) that densities in the range 3×10^{10} to $3\times10^{11}\mathrm{cm}^{-3}$ give agreement with the observations. Changing the field ratios has only a small effect on the shape of the curves. This is because the $d\ln B/dS$ pitch-angle change is not itself position-dependent but feeds back into the positional dependence via the first of Eq. 5, unlike the case of chromospheric convergence where $d\ln B/dS$ is strongly dependent on position.

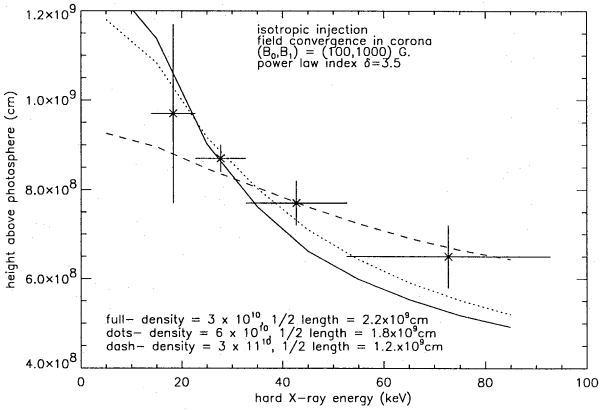

Fig. 12. All field convergence takes place in the corona. The curves correspond to three different density values.

6. Distinguishing between various models

There are many variable parameters in this treatment and evidently a limit to the information yielded by modeling the single set of observations considered here. We have seen that a wide variety of beam and atmosphere parameters can reproduce the height-versus energy distribution observed. We therefore suggest some further tests to tie down better these parameters. It is possible using work already published to predict certain behaviours, but detailed calculations will be presented in a subsequent paper.

The distribution of X-ray intensity with position depends in our model on loop density, electron angular distribution, and magnetic field. For example, we have found using the stochastic method and studying the spatial distribution of HXR emission (Fletcher 1995), that because of transport effects, a patch of HXR emission (feinter than the footpoint emission) is present at the top of the loop, with size, and intensity dependent on loop density and beam angular injection pattern. For individual well observed loops, calculations of the distribution may be compared with HXT observations. For example, it is demonstrated in Fletcher (1995) that an increase in loop density leads to an increase in the ratio of looptop to footpoint emission intensity, and shrinking of the source.

Were suitable instruments to become available, studies of X-ray linear polarization would be useful. If one were able to observe polarization from limb flares, uncontaminated by backscattered photospheric X-rays (as footpoint sources would be) this would reflect directly the angular and energetic distribution of electrons near the point of injection. For example, Haug (1972) has shown that a distribution which is peaked along the field ($f(\alpha) \propto \sin\alpha$) gives a large positive polarization (perpendicular to plane of magnetic field and photon) if viewed at 90° to the field direction, whereas a distribution peaked perpendicular to the field gives a large negative polarization (parallel to plane of magnetic field and photon directions). An isotropic distribution will give zero polarization. In addition the degree

of polarization varies with photon energy, decreasing as photon energy increases.

We may be able to glean some information on the nature of the magnetic field by studying the distribution of HXR bursts across the solar disc. It was proposed by MacKinnon & Brown (1990) that the anisotropy of $>$ 10 MeV flare γ - ray bursts could be explained by a combination of increasing density and strong field convergence in the chromosphere. The basic argument is that strongly beamed γ-ray bremsstrahlung emission is only visible when the emitting electrons are moving towards the observer, and assuming that the bulk of the emission comes from the chromosphere, where the net field is locally vertical, limb-flare electrons whose emission we see must be moving perpendicular to the field, because of either scattering or mirroring. Roughly speaking they found that magnetic fields which converge weakly, high in the chromosphere resulted in more anisotropic distributions than those which converged strongly low in the chromosphere. Although for X-rays the emission pattern is not so strongly beamed (an opening angle of about 50° at 50keV, compared to 3° at 10MeV) resulting in a far more isotropic burst distribution, we would still expect to find some dependence on field shape which, with the much larger amount of available data on HXR bursts, may yet give some indication as to the field convergence. For example, we expect that a field which converges mostly in the corona would give a more anisotropic footpoint HXR distribution than one which converges low in the chromosphere, since in the former case fewer electrons will mirror in the dense chromosphere and emit line-of-sight radiation from the limb than in the latter case. However one other important factor is in the difference in collisional stopping depth of 100keV and 10MeV electrons. This means that results of MacKinnon & Brown (1990) cannot be directly taken applied to the lower energy case, and a full calculation is demanded.

7. Discussion and conclusions

The results presented above suggest that an impulsive flare model in which energetic electrons are accelerated into a coronal magnetic loop in which they scatter and mirror is capable of explaining the height with energy variation of HXR sources observed by the HXT onboard Yohkoh. This model makes certain testable predictions. Firstly, the emission spectrum at high energy (so with no thermal contamination) will have a softer spectrum at the top of the loop than at the bottom. Secondly, because of transport effects we find that a bright patch of HXR emission will be situated at the top of the loop (Fletcher 1995). Thirdly, if observed, HXR polarization from the source would decrease in magnitude as one progresses down the loop, as the electron distribution isotropises.

In keeping our model simple we have not considered the effect of non-uniform coronal density. Gravitational stratification will be minimal due to the large coronal scale height, however phenomona such as overdensity at the top of loops could have an effect. There are some observational suggestions that gas at loop tops emits more brightly in SXR than that in the rest of the loop (Dennis et al. 1994), implying a density of as much as $1.2 \times 10^{12}\mathrm{cm}^{-3}$, occupying a volume of 2.2×10^{27} cm^{-3} (a sphere 2 Soft X-ray Telescope pixels in radius) might be present This gas would present a column of $2.2 \times 10^{20}\mathrm{cm}^{-2}$. Although hot, it would be a 'cold-target' to HXR emitting electrons, in which they would suffer collisional losses, altering the final HXR emission versus height. The effect would, on average, be to shift the distribution upwards and flatten the gradient. Note that this quoted high density is the highest inferred, normal values being around $3 \times 10^{11}\mathrm{cm}^{-3}$. In addition to its effect on the propagation of non-thermal electrons, thermal X-radiation would be emitted from such a source, however the SXR temperatures observed, of $\sim 2 \times 10^7$ K would result only in significant changes to the curve at low energies ($\lesssim$ 10keV) but where there is considerable leeway in the error bar in any case.

There are 2 other data points not shown on our graphs - those provided by Kane (1983) and Takakura et al. (1986). The measurement of Takakura et al. has associated with it error bars large enough to encompass all the models here presented, and unfortunately the statistics on the bins at $\sim$ 150keV are too poor to permit a meaningful comparison with the Kane et al. (1983) data point. Modelling electrons of this energy at the same time as low energy electrons would require either an increase in the number of particles run through the code, and the run time, by a factor of at least 10, or implementation of a 'splitting' scheme (e.g., Yoshida and Yanagita, 1994) to artificially increase the number of high energy computational particles.

As mentioned in Sect. 1.2, a shortcoming of our modelling is that we have not included the effect on the beam of a return current, although we have given some justification for this. However it is instructive to consider the effect of its inclusion. In general, the inclusion of a return current inhibits the downwards progress of the beam electrons, following from which it is expected that the site of non-thermal emission tends towards higher altitudes. This was pointed out by Knight and Sturrock (1993) and substantiated by the calculations of McClements (1992), who finds that the chromospheric component is reduced compared to the no-return-current case. The coronal intensity is found to be more-or-less unaffected by the return current. McClements considers only a single energy of HXR emission, and to see the effect of return current losses on particles of different energies we refer to Emslie (1980) who finds the following result for the reverse current energy losses for a power-law spectrum of electrons.

$$dE/dN(S)_r = \frac{\eta e^2}{n}\left(1 + \frac{E^*}{E_o}\right)^{(1-\delta)} \qquad (15)$$

where $N(S)$ is the column depth, and E^* the injection energy necessary to reach N with $E = 0$. So as $N(S)$ increases, E^* increases and $dE/dN(S)_r$ decreases. Therefore in addition to an increase overall in the height of HXR emission, we would expect the curve to steepen, since dE/dN is greater for low energy electrons which spend most of their lifetimes at low N than it is for high energy electrons, which spend more of their time at high N and n. Note that the $1/n$ term in (15) means that return current losses are not so important in high density cases.

In conclusion we state that the height-versus-energy distribution of hard X-rays averaged over 92 flares observed by Yohkoh, can be successfully reproduced by a non-thermal model, in which accelerated electrons are partially trapped in a coronal magnetic bottle. To fit the data we require loops of density $2 \times 10^{10} - 3 \times 10^{11} \mathrm{cm}^{-3}$ and length $1.3 - 2.8 \times 10^{9} \mathrm{cm}$, which are perfectly reasonable flare loop values. We find that a large range of values of loop length, density, and beam parameters can give an acceptable fit, but most of these factors can be obtained by observation. To aid in distinguishing between the allowable models, we have suggested a number of possible independent tests, results of which will appear in a subsequent paper.

Acknowledgements. It is with pleasure that I thank J. Kuijpers of the Sterrekundig Instituut Utrecht and N. Vilmer and G.Trottet of the Observatoire de Meudon for useful discussion and acknowledge the support of E.C. Lab-Twinning Contract number SCI*-CT91-0727. The useful comments of Dr. T. Kosugi and an anonymous referee are also gratefully acknowledged.

References

Alexander, D., 1990, A&A 235, 431
Brown, J.C., McClymont, A.N., 1975, Sol.Phys. 41,135.
Dennis, B.R., Holman, G.D., Hudson, H.S., et.al., 1994. Flares. In: S. Enome and T. Hirayama (eds) NRO Report no. 360, Proceedings of the Kofu Symposium, Radioheliograph Series, p.217
Doschek, G., 1994. Flares. In: S. Enome and T. Hirayama (eds) NRO Report no. 360, Proceedings of the Kofu Symposium, Radioheliograph Series, p173.
Emslie, A.G., 1978, ApJ 224, 241.
Emslie, A.G., 1980, Ap.J 235, 1055.
Fletcher, L., Brown, J.C., 1995, A&A 296, 260.
Fletcher,L., 1995 A&A Lett., 303, L9
Gardiner, C.W., 1985. In H.Haken (ed.), Handbook of Stochastic Methods
Hamilton, R.J., Lu, E.T., Petrosian V., 1990, ApJ 354, 726.
Haug,E., 1972, Sol.Phys. 25, 425.
Hulot, E., Vilmer, N., Chupp, E.L., et al., 1992, A&A 256, 273.
Kosugi, T., Makishima, K., Murakami, T., et al., 1991, Sol. Phys. 136, 17.
Kane, S.R., 1974. In G. Newkirk (ed) 'Coronal Disturbances', IAU Symp. 57, p.105.
Kane, S.R., 1983, Sol. Phys. 86, 355
Karlickỳ, M., Alexander, D., Brown, J.C., et al., 1990, Sol. Phys. 129, 325.
Knight, J.W., Sturrock, P.A., 1977, ApJ 218, 306.
Leach, C.F., Petrosian, V., 1981, ApJ 251, 781
Machado, M., Avrett, E.H., Vernazza, J.E., Noyes, R.W., 1980, ApJ 242, 336
McClements, K.G., 1990, A&A 234, 487.
McClements, K.G., 1992, A&A 258, 542.
MacKinnon, A.L., 1988, A&A 194, 279
MacKinnon, A.L., Brown, J.C., 1989, A&A 215,371
MacKinnon, A.L., Brown, J.C., 1990, A&A 232, 544.
MacKinnon, A.L., Craig, I.J.D., 1991, A&A 251, 693.
Mandzhavidzhe, N., Ramaty, R., 1993, Nuclear Physics B (Proc. Suppl.), 33, 141.
Matsushita, K., Masuda, S., Kosugi,T., Inda, M., Yaji, K., 1992, PASJ, 44, L89.
Melrose, D.B., Brown, J.C., 1976, MNRAS, 176, 15
van den Oord, G.H.J., 1990, A&A 234, 496.
Ogawara, Y., Takano, T., Kato, T., et al., 1991, Sol. Phys. 136
Sakao, T., 1994, Ph.D. Thesis, University of Tokyo.
Sakao, T., Kosugi, T., Masuda, S., et al., 1994. Flares. In: S. Enome and T. Hirayama (eds), NRO Report no. 360, Proceedings of the Kofu Symposium, Radioheliograph series p.169
Solanki S.K., Steiner, O., 1990, A&A 234, 519
Takakura, K., Tanaka, K., Hiei, E., 1984, Adv.Sp.Res. 4, 143
Takakura, K., Tanaka, K., Nitta, N., Kai, K., Ohki, K., 1986, Sol. Phys. 107, 109.
Vlahos, L., Machado, M.E., Ramaty, R., et al., 1984, Particle acceleration. In: NASA Conf.Publ. 2439, "Energetic Phenomena on the Sun - Proceerings of the SMM Flare Workshop", Greenbelt USA, p..
Yoshida, T., Yanagita, S.,1994, Prog.Theor.Phys. 92, 1217.

This article was processed by the author using Springer-Verlag LaTeX A&A style file version 3.